OPEN

Tuning electronic and optical properties of monolayer PdSe$_2$ by introducing defects: first-principles calculations

X. W. Zhao[1], Z. Yang[1], J. T. Guo[1], G. C. Hu[1], W. W. Yue[1], X. B. Yuan[1]* & J. F. Ren[1,2]*

Based on the density functional theory, the electronic and optical properties of pristine monolayer PdSe$_2$ with Pd or Se vacancy-defect are investigated. Our results show that the Se defect is energetically more favorable than that of Pd defect. The band gap reduces, and some new midgap states appear after the Pd or Se defects are introduced. In terms of the optical properties, the prominent anisotropic characters are remained. The obvious new peaks of the dielectric constant appear after introducing defects. The light absorption in the visible energy range expands based on the appearance of the midgap states induced by the Pd or Se defects. The changes of the refractive index and reflectivity are similar with those of the dielectric constants and the light absorption. The energy loss spectrum of the PdSe$_2$ with Pd or Se defects is obviously different, which can be used to identify different defects in PdSe$_2$. These findings provide effective strategies to tune electronic and optical properties of monolayer PdSe$_2$ by introducing defects.

In the last decades, the successful stripping of graphene greatly stimulates people's interest in the study of two-dimensional (2D) materials[1–5]. However, the zero-band gap of graphene limits its applications in electronics, which leads to the emergence of other 2D materials beyond graphene, such as black phosphorous, boron nitride and transition metal di-chalcogenides (TMDCs)[6–11]. The common formula for TMDCs is MX$_2$, where the M and X represent transition metals and chalcogen, respectively[12]. The favorable band-gap phenomenon together with the excellent chemical properties of TMDCs enable a wide range of application prospects in field-effect transistors, energy storage, catalysis, and so on[10,11]. Besides, several TMDCs have been widely studied both theoretically and experimentally based on their distinguished mechanics, electronics and optical properties, such like MoS$_2$, MoSe$_2$, and WS$_2$[13–15]. Recently, another class of layered materials formed by noble metals (e.g. Pd and Pt) with S or Se atoms have been widely investigated owing to their unique atomic and electronic structures[16,17].

Monolayer PdSe$_2$, which is a special 2D material, possesses an uncommon pentagonal structure. Pd atoms coordinate with four Se atoms to form a square backbone network. Monolayer PdSe$_2$ has been successfully exfoliated by Akinola D. Oyedele *et al.* for the first time, which provides exciting opportunities for the research of pentagonal 2D materials[18]. The air-stability and anisotropy of monolayer PdSe$_2$ have been proved, moreover, few-layered PdSe$_2$ behaves ambipolar semiconducting with high electron-apparent field-effect mobility. In addition, the remarkable electronic structures of PdSe$_2$ are layer-dependent. The monolayer PdSe$_2$ has an indirect band gap about 1.43 eV, while bulk PdSe$_2$ has a band gap of 0.03 eV[18,19]. The promising thermoelectric performance of monolayer PdSe$_2$ has been demonstrated through the density functional theory and semiclassical Boltzmann transport equation by Dan Qin *et al.* as well[20]. Overall, the discovery of pentagonal PdSe$_2$ makes the emerging physics related to such low-symmetry structure possible. What's more, monolayer PdSe$_2$ can be a promising candidate in the applications of piezoelectrics, valleytronics, optoelectronic and spintronics.

In order to effectively optimize and utilize the excellent properties of 2D materials, various strategies to tune the optical and electronic properties of 2D materials have been adopted, such as the introduction of defects[21], electric field and strain modulation[19,22], atom doping and adsorption[23,24], strain engineering[25] etc. As we all know, defects can tune the electronic[26], magnetic[27], optical properties and enhance the electrochemical activity[19,28]. The

[1]School of Physics and Electronics, Shandong Normal University, Jinan, 250014, China. [2]Shandong Provincial Engineering and Technical Center of Light Manipulations & Institute of Materials and Clean Energy, Shandong Normal University, Jinan, 250014, China. *email: yxb@sdnu.edu.cn; renjf@sdnu.edu.cn

existence of the point defects in semiconductors can efficiently trap free electrons, holes and localize excitons. When it recombines radiatively, the excitons can lead to light emission at energies lower than the band-to-band optical transition energy. On account of tighter localization of the electron wavefunction, the interactions between the defects and excitons become stronger in reduced dimensionalities materials[29]. On one hand, for monolayer $PdSe_2$, it is highly desirable to explore the optical and electronic properties and develop simple and effective strategies to improve them. This will not only help to enhance the performance of device dependent on monolayer $PdSe_2$ but also contribute to its applications in nanoelectronic devices. On the other hand, Lin *et al*. have reported that they have synthesized a novel 2D material monolayer Pd_2Se_3, which is a fusion of two defective $PdSe_2$ layers due to the Se vacancies with a certain concentration[30,31]. They have systematically stated that the monolayer Pd_2Se_3 has excellent anisotropic electronic and optical properties and is a very promising candidate for photovoltaics. Take these things into account, we can infer that it is valuable to investigate the effects of the defects on the electronic and optical properties of $PdSe_2$. In this work, we perform the first-principles calculations to investigate the electronic and optical properties of monolayer $PdSe_2$ with Pd or Se vacancy defects, the Pd or Se defects are introduced by the random elimination of atoms. After introducing defects, obvious changes for electronic and optical properties of $PdSe_2$ can be obtained.

Results and Discussions

Firstly, the structural parameters of $PdSe_2$ monolayer, $PdSe_2$ with Pd or Se defects are calculated. The bond lengths and angles of vacancy-defected $PdSe_2$ have little changes compared with the primitive cell, which means that there is only a slight distortion of the system, so the $PdSe_2$ with a Pd or Se defect is stable. In order to further compare these two defects, the formation energies are obtained through the following equation $E_{form} = E_{defect} - E_{pristine} \pm \mu_n$, where E_{defect} represents total energies of the relaxed $PdSe_2$ with Pd or Se defect, $E_{pristine}$ is the energy of the pristine $PdSe_2$, μ_n is the chemical potential of the Pd or Se atom defect. The more positive the E_{form} is, the more difficult the defect to be formed. From our calculations, it can be obtained that the E_{form} of $PdSe_2$ with Se defect is 1.38 eV, while for the $PdSe_2$ with Pd defect, it is 1.97 eV, so Se defect is the more energetically favorable type. Recent work also has experimentally demonstrated the presence of Se defect in $PdSe_2$[32].

To further clarify the effects of defect on the electronic properties of monolayer $PdSe_2$, the band structures along high symmetry k-points are depicted in Fig. 1. Figure 1(a–c) represent the band structures with PBE, Fig. 1(d–f) represent the band structures based on HSE06, respectively. By contrast, it can be found that the PBE underestimates the band gap, the HSE06 is more reasonable to calculate the electronic and optical properties, so the HSE06 are adopted in all the following calculations. As shown in Fig. 1(d), the pristine structure of monolayer $PdSe_2$ has an indirect band gap about 2.25 eV, which is consistent with previous work[33]. However, after introducing Pd or Se defects, the band gaps are 1.45 and 1.91 eV, respectively. It can be observed from Fig. 1(e,f) that the presence of Pd or Se defect leads to some different new midgap states within the energy band gap, which can also be identified by the sharp peaks in the density of states. All the systems remain indirect band gap, and the $PdSe_2$ with Pd defect still shows semiconductor characteristics. For the $PdSe_2$ with Se defect, the band of midgap state goes through the Fermi level, the $PdSe_2$ shows metal characteristics. It is also indicated that introducing defects is a potentially useful strategy to tune the band gap of 2D materials.

The total density of states (TDOS) and projected density of states (PDOS) for pristine $PdSe_2$, $PdSe_2$ with Pd or Se defect are shown in Fig. 2. For pristine $PdSe_2$, it can be found that the dx_2, dxy orbital of Pd atoms and the px, pz orbital of Se atoms mainly contribute to the states at conduction band edge, the dz^2 orbital of Pd atoms and the px, pz orbital of Se atoms mainly contribute to the valence band edge. Besides, there is significant hybridization between Pd d and Se p states. While after introducing the defects, there are some changes, as shown in Fig. 2(b,c). It is obvious that the midgap states are mainly originated from the p^x and pz orbital of Se atoms in $PdSe_2$ with Pd defect, while for $PdSe_2$ with Se defect, the midgap states mainly originate from dx^2 and dxy orbital. In general, the appearance of the peaks in the gapped region of the DOS are associated with the midgap states localized around the defects, which arises from the dangling bonds of Pd or Se due to their unsaturated charges, and their strength depends on the different missing atoms[34]. Thus one can identify the types of defect through the PDOS and then characterize the $PdSe_2$ in order to get expected electronic properties.

Optical properties of the materials are closely connected to its electronic properties. And it is evident from the previous calculations that the defects can alter the electronic properties of monolayer $PdSe_2$, the change of electronic properties is expected to modify the optical properties. Figure 3(a–c) represent the real parts of the dielectric constant ε_1 for pristine $PdSe_2$, $PdSe_2$ with Pd or Se defect, (d)–(f) represent the corresponding imaginary parts ε_2, respectively. From Fig. 3(a–c), it can be found that the maximum value of ε_1 in x direction for pristine $PdSe_2$ is about 7.62, however, it reduces to 6.94 and 4.15 for $PdSe_2$ with Pd or Se defect, respectively. The maximum values are 7.06, 6.41 and 4.02 for pristine $PdSe_2$, $PdSe_2$ with Pd or Se defect in y direction of ε_1, which is different from those in x direction. After introducing defect, the maximum value of ε_2 also decreases from 6.03 for pristine $PdSe_2$ to 5.39 and 3.36 for $PdSe_2$ with Pd or Se defect in x direction, respectively. It can be found that the change of ε_2 is different as well both in x and y directions, which means that the anisotropy of the optical properties of $PdSe_2$ remains unchanged. Furthermore, the peaks in the low energy range of dielectric constant correspond to the peaks in the DOS, which mainly due to the new midgap states originated from the defects.

The absorption coefficients $\alpha(\omega)$ for pristine $PdSe_2$, $PdSe_2$ with Pd or Se defect have been depicted to reveal the light absorption properties of $PdSe_2$, which are shown in Fig. 4. The optical absorption spectrum is closely related to the imaginary parts of the dielectric constant. It can be observed that there is no absorption within the energy range of 0 to 2.20 eV for pristine $PdSe_2$ as shown in Fig. 4(a), which is consistent with the band gap structure in Fig. 1(d). According to the suitable band gap, monolayer $PdSe_2$ is expected to be a promising candidate for light absorption. Monolayer $PdSe_2$ exhibits good optical absorption in the visible regions (1.64–3.19 eV) as is shown in Fig. 4(a). After introducing the Pd or Se defect, the absorption is optimized obviously. The optical absorption starts from 0.44 and 0.53 eV for the $PdSe_2$ with Pd or Se defect, which are shown in Fig. 4(b,c). That is to say, the
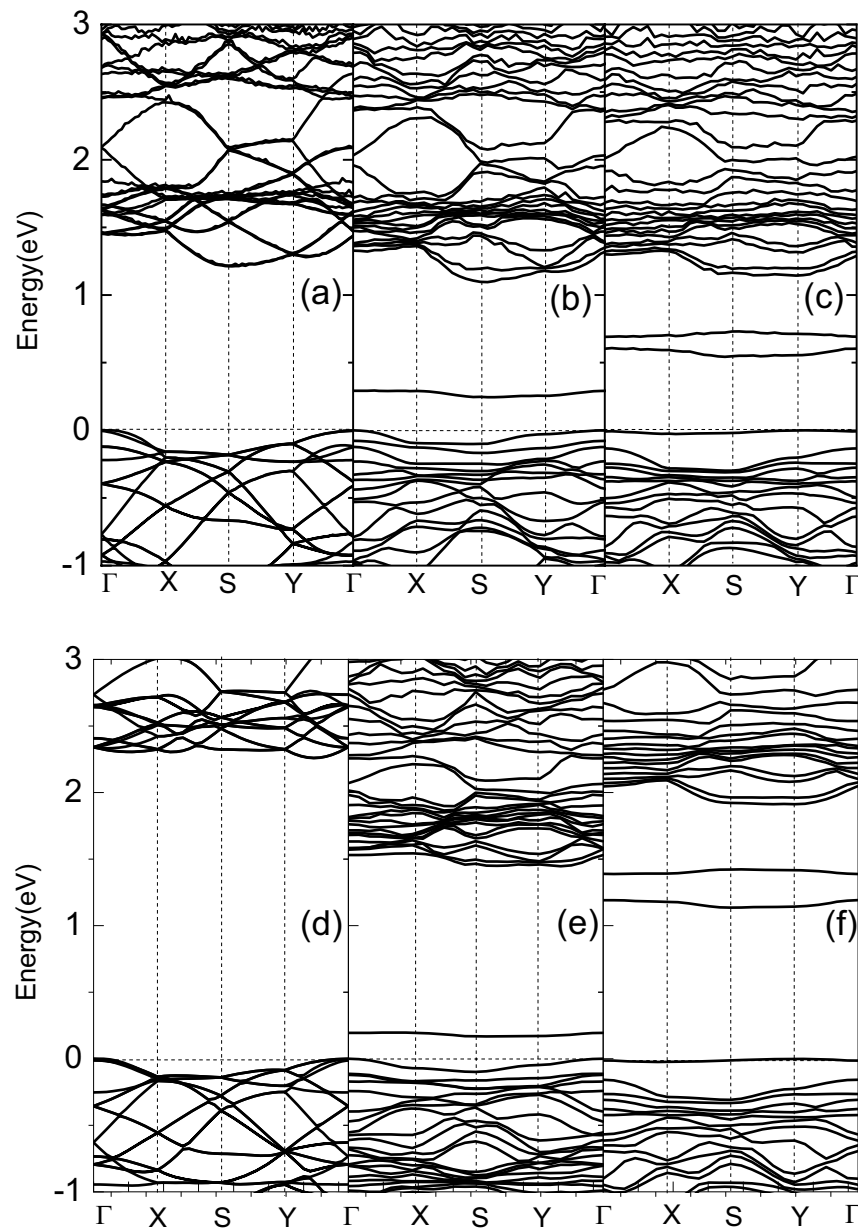
Figure 1. Band structures with PBE for pristine $PdSe_2$ (**a**), $PdSe_2$ with Pd defect (**b**) and Se defect (**c**), respectively. (**d–f**) Correspond to the cases with HSE06.

optical absorption in low energy region widens, especially in the visible regions. That is benefit from the existence of the Pd or Se defect in $PdSe_2$, they can create some midgap states, so more new optical transitions can be activated comparing with the case of pristine $PdSe_2$. In addition, it can be found that the absorption coefficients are different in x and y directions.

Figure 5 shows the refractive index $n(\omega)$ and reflectivity $R(\omega)$ of $PdSe_2$ systems. The maximum value of $n(\omega)$ for pristine $PdSe_2$ is about 2.82. There is noticeable change for the maximum $n(\omega)$ of the $PdSe_2$ with Pd or Se defect compared with that of pristine $PdSe_2$, it decreases to 2.72 and 2.01. And the new peak of $n(\omega)$ appears in low energy region obviously as shown in Fig. 5(b,c), which is consistent with the dielectric constant. The $R(\omega)$ of $PdSe_2$ systems are shown in Fig. 5(d–f) respectively. The maximum $R(\omega)$ for the pristine $PdSe_2$ and $PdSe_2$ with Pd or Se defects are 0.32, 0.25 and 0.17, respectively. It is obvious that the maximum $R(\omega)$ decreases compared with that in pristine $PdSe_2$, and there are new peaks in low energy region after introducing Pd and Se defects. All the new peaks in low energy region are related to the new midgap states.

The electron energy loss spectrum $L(\omega)$ have also been depicted for pristine $PdSe_2$, $PdSe_2$ with Pd or Se defect, which are shown in Fig. 6(a–c), respectively. By contrast, it can be found that obvious differences occurred due to the introduction of the defects. The $L(\omega)$ starts from 2.31, 0.31 and 0.45 eV for pristine $PdSe_2$, $PdSe_2$ with Pd or Se defect, respectively. The first sharp peak of $L(\omega)$ is observed at 5.13, 1.75 and 0.68 eV. Besides, the curves of pristine $PdSe_2$ and $PdSe_2$ with Se defect have a tendency of ascending first and descending in succession then
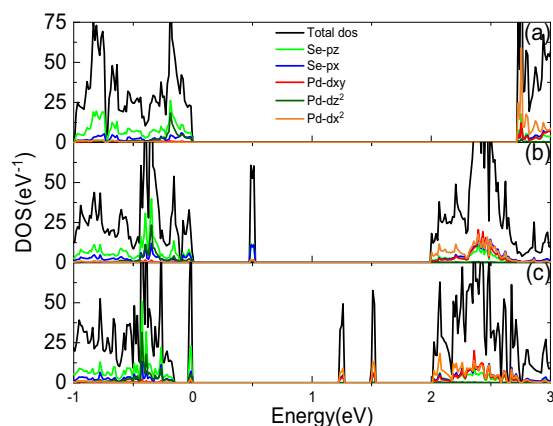
Figure 2. Density of states for different systems. (**a–c**) correspond to pristine PdSe$_2$, PdSe$_2$ with Pd or Se defect, respectively.
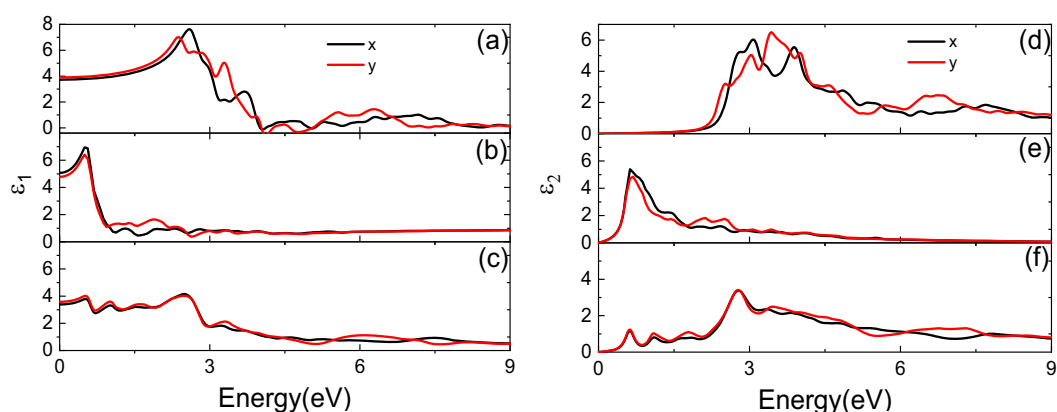
Figure 3. Dielectric constant of monolayer PdSe$_2$. (**a–c**) Are the real part of dielectric function ε_1 for pristine PdSe$_2$, PdSe$_2$ with Pd and Se defect, (**d–f**) Correspond to the imaginary parts ε_2.
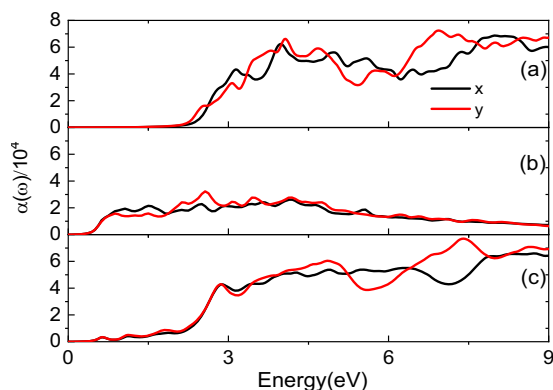

Figure 4. Absorption coefficient for pristine PdSe$_2$ (**a**), PdSe$_2$ with Pd (**b**) and Se defect (**c**), respectively.

ascending. While the curve of PdSe$_2$ with Pd defect has a tendency of ascending first and descending in succession, and it has relatively dense peaks. The different $L(\omega)$ can be used to identify different defects.

Conclusions

In this work, the electronic and optical properties of pristine PdSe$_2$, PdSe$_2$ with Pd or Se defect are studied through the first-principles calculations based on the density functional theory. The result of the formation energies indicates that Se defect is more energetically favorable compared with that of Pd defect. By calculating the band structures, it is found that the band gap reduces due to the appearing of the new midgap states after introducing Pd or
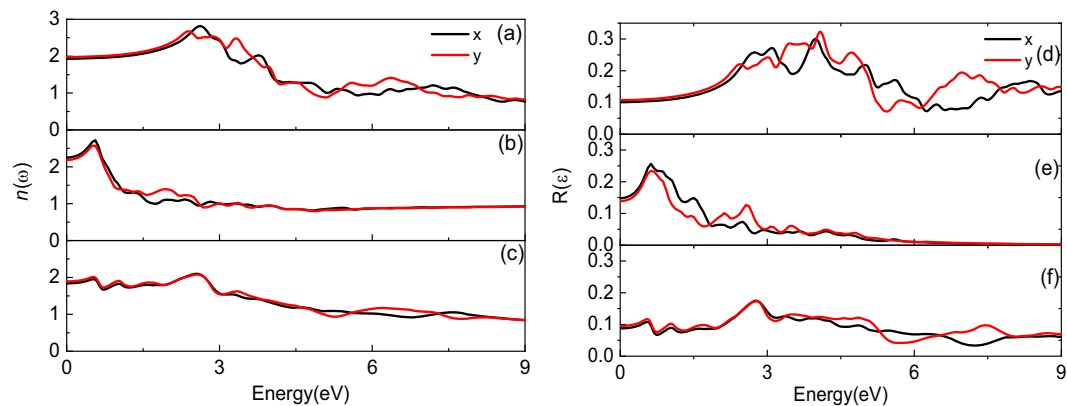
Figure 5. Refractive index and reflectivity of PdSe$_2$ systems. (**a–c**) Correspond to refractive index, (**d–f**) correspond to reflectivity for pristine PdSe$_2$, PdSe$_2$ with Pd or Se defect, respectively.
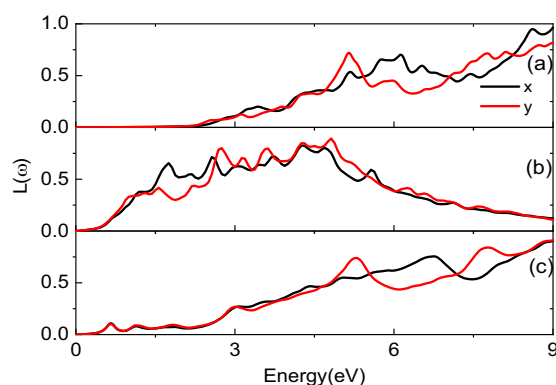

Figure 6. Electron energy loss spectrum for pristine PdSe$_2$ (**a**), PdSe$_2$ with Pd (**b**) or Se defect (**c**), respectively.

Se defect. The midgap states are originated from the dangling bonds of Pd or Se due to their unsaturated charges. In terms of the optical properties, the dielectric constant and absorption spectrum, refractive index, reflectivity and electron energy loss spectrum have been analyzed. The obvious peaks of the dielectric constant and the absorption spectrum in low energy region can be observed due to the appearance of the new midgap states induced by the Pd or Se defect. And the prominent anisotropic characters are remained. The light absorption area in the visible regions widens after introducing Pd or Se defect compared with that of pristine PdSe$_2$. The new peaks benefit from the appearance of the midgap states which activate more new optical transitions in the optical spectrum. For the refractive index and reflectivity, the similar changes have been taken place. Furthermore, the difference of the electron energy loss spectrum can be used to identify different defects. All these findings provide effective strategies to tune electronic and optical properties of monolayer PdSe$_2$, and provide possibilities for monolayer PdSe$_2$ in the applications of optoelectronics.

Theoretical model and computational details. All our theoretical calculations are performed through VASP (Vienna ab-initio Simulation Package)[35,36], PAW pseudopotential is used to describe the interaction between ions and electrons[37,38]. In terms of the energy exchange correlation energy function, the generalized gradient approximation (GGA) in the form of Perdew-Burke-Ernzerhof (PBE) is used[39]. The electronics and optical properties are calculated by the hybrid functional based on the Heyd-Scuseria-Ernzerhof (HSE06) exchange-correlation functional[40]. The cut-off energy is 400 eV in the process of the structural optimizations and calculations. The $11 \times 11 \times 1$ Monkhorst-Pack grid is chosen when calculating the integral in Brillouin zone. Energy convergence is set to less than 10^{-4} eV and the convergence accuracy of the nuclear motion is set to less than 0.01 eV/Å. A $3 \times 3 \times 1$ supercell (54 atoms) of PdSe$_2$ is constructed, as shown in Fig. 7. It is worth noting that the residual strain may exist due to the limit of periodic boundary condition no matter how bigger the supercell is. In order to avoid the interlayer interference, the thickness of the vacuum layer is set to 20 Å.

The optical properties are general evaluated by the dielectric function which are the sum of real and imaginary parts, $\varepsilon(\omega) = \varepsilon_1(\omega) + i\varepsilon_2(\omega)$. The imaginary part is calculated by the summation of empty band states using the following equation[41],
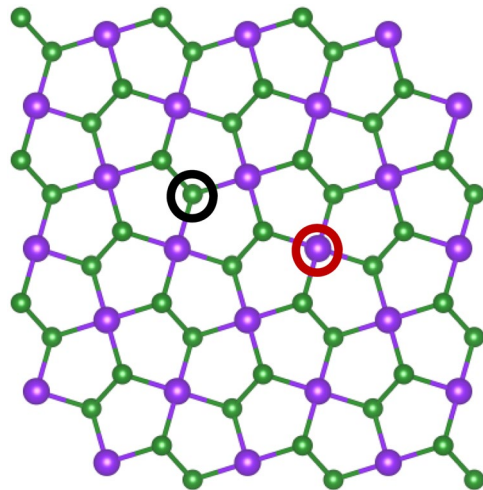
Figure 7. Top view of PdSe$_2$ monolayer. Green and purple spheres represent Se and Pd atoms, red and black circle represent Pd and Se vacancy-defect positions, respectively.

$$\varepsilon_2(\omega) = \frac{4\pi^2 e^2}{\Omega} \lim_{q \to 0} \frac{1}{q^2} \sum_{c,v,k} 2\omega_k \delta(\in_{ck} - \in_{vk} - \omega) \times \left\langle u_{ck+e_\alpha q}|u_{vk}\right\rangle \left\langle u_{ck+e_\beta q}|u_{vk}\right\rangle^* \tag{1}$$

where Ω represents the volume, v and c correspond to the valence and the conduction band respectively, α and β indicate the Cartesian components, e_α and e_β are the unit vectors, $\in_{ck}$ and $\in_{vk}$ refer to the energy of conduction and valence band respectively, u_{ck} is the cell periodic part of the orbitals at the k-point. The real part of dielectric constant is calculated by the Kramers-Kronig relation[42]

$$\varepsilon_1(\omega) = 1 + \frac{2}{\pi} P \int_0^\infty \frac{\varepsilon_2^{\alpha\beta}(w')w'}{w'^2 - w^2 + i\eta} d\omega', \tag{2}$$

with P being the principle value. According to the values of real and imaginary part of the dielectric constant, the optical absorption coefficient $\alpha(\omega)$, the refractive index $n(\omega)$, the reflectivity $R(\omega)$, and the electron energy loss spectroscopy $L(\omega)$ can be given by[43],

$$\alpha(\omega) = \frac{\sqrt{2}\,\omega}{c}\left\{\left[\varepsilon_1^2(\omega) + \varepsilon_2^2(\omega)\right]^{\frac{1}{2}} - \varepsilon_1(\omega)\right\}^{\frac{1}{2}}, \tag{3}$$

$$n(\omega) = \frac{1}{\sqrt{2}}\left\{\left[\varepsilon_1^2(\omega) + \varepsilon_2^2(\omega)\right]^{\frac{1}{2}} + \varepsilon_1(\omega)\right\}^{\frac{1}{2}}, \tag{4}$$

$$R(\omega) = \left|\frac{\sqrt{\varepsilon_1(\omega) + i\varepsilon_2(\omega)} - 1}{\sqrt{\varepsilon_1(\omega) + i\varepsilon_2(\omega)} + 1}\right|^2, \tag{5}$$

$$L(\omega) = \frac{\varepsilon_2(\omega)}{\varepsilon_1^2(\omega) + \varepsilon_2^2(\omega)}. \tag{6}$$

References

1. Novoselov, K. S. *et al.* Electric field effect in atomically thin carbon films. *Sci.* **306**, 666–669, https://doi.org/10.1126/science.1102896 (2004).
2. Zhang, Y., Small, J. & Kim, P. Electric field modulation of galvanomagnetic properties of mesoscopic graphite. *Phys. Rev. Lett.* **94**, 176803, https://doi.org/10.1103/physrevlett.94.176803 (2005).
3. Cai, W. *et al.* Graphene saturable absorber for diode pumped Yb:Sc$_2$SiO$_5$ mode-locked laser. *Opt. Laser. Technol* **65**, 1–4, https://doi.org/10.1016/j.optlastec.2014.06.010 (2015).
4. Yuan, X. B. *et al.* Spin polarization properties of benzene/graphene with transition metals as dopants: First principles calculations. *Appl. Surf. Sci.* **439**, 1158–1162, https://doi.org/10.1016/j.apsusc.2018.01.180 (2018).

5. Yuan, X. B., Yang, M. S., Tian, Y. L., Cai, L. L. & Ren, J. F. Spin polarization properties of thiophene molecule adsorbed to the edge of zigzag graphene nanoribbon. *Synthetic Met.* **226**, 46–49, https://doi.org/10.1016/j.synthmet.2017.01.013 (2017).

6. Warner, J. H., Rummeli, M. H., Bachmatiuk, A. & Buchner, B. Atomic resolution imaging and topography of boron nitride sheets produced by chemical exfoliation. *ACS Nano* **4**, 1299–1304, https://doi.org/10.1021/nn901648q (2010).

7. Watanabe, K., Taniguchi, T. & Kanda, H. Direct-bandgap properties and evidence for ultraviolet lasing of hexagonal boron nitride single crystal. *Nat. Mater* **3**, 404–409, https://doi.org/10.1038/nmat1134 (2004).

8. Li, L. *et al.* Black phosphorous field-effect transistors. *Nat. Nanotechnol.* **9**, 372–377, https://doi.org/10.1038/nnano.2014.35 (2014).

9. Xia, F., Wang, H. & Jia, Y. Rediscovering black phosphorous as an anisotropic layered material for optoelectronics and electronics. *Nat. Commun* **5**, 4458, https://doi.org/10.1038/ncomms5458 (2014).

10. Jariwala, D., Sangwan, V. K., Lauhon, L. J., Marks, T. J. & Hersam, M. C. Emerging device applications for semiconducting two-dimensional transition metal dichalcogenides. *ACS Nano* **8**, 1102–1120, https://doi.org/10.1038/ncomms5458 (2014).

11. Miro, P., Audiffred, M. & Heine, T. An atlas of two-dimensional materials. *Chem. Soc. Rev.* **43**, 6537–6554, https://doi.org/10.1039/C4CS00102H (2014).

12. Sun, J. F., Shi, H. L., Siegrist, T. & Singh, D. J. Electronic, transport, and optical properties of bulk and mono-layer $PdSe_2$. *Appl. Phys. Lett.* **107**, 153902, https://doi.org/10.1063/1.4933302 (2015).

13. Ahmed, S. *et al.* Inducing high coercivity in MoS_2 nanosheets by transition element doping. *Chem. Mater.* **29**, 9066–9074, https://doi.org/10.1021/acs.chemmater.7b02593 (2017).

14. Qiu, B. *et al.* Tuning optical properties of graphene/WSe_2 heterostructure by introducing vacancy: First Principles Calculations. *Physica E* **116**, 113729, https://doi.org/10.1016/j.physe.2019.113729 (2020).

15. Chen, Y., Gan, L., Li, H., Ma, Y. & Zhai, T. Achieving uniform monolayer transition metal dichalcogenides film on silicon wafer via silanization treatment: A typical study on WS2. *Adv. Mater.* **29**, 1603550, https://doi.org/10.1002/adma.201603550 (2017).

16. Ahmad, S. Strain dependent tuning electronic properties of noble metal di chalcogenides pdx$_2$ (x = s,se) monolayer. *Mater. Chem. Phys.* **198**, 162–166, https://doi.org/10.1016/j.matchemphys.2017.05.060 (2017).

17. Chow, W. L. High mobility 2d palladium diselenide field-effect transistors with tunable ambipolar characteristics. *Adv. Mater.* **29**, 14090–14097, https://doi.org/10.1002/adma.201602969 (2017).

18. Oyedele, A. D. *et al.* $PdSe_2$: pentagonal two-dimensional layers with high air stability for electronics. *J. Am. Chem. Soc.* **139**, 14090–14097, https://doi.org/10.1021/jacs.7b04865 (2017).

19. Deng, S., Li, L. J. & Zhang, Y. Strain modulated electronic, mechanical, and optical properties of the monolayer PdS_2, $PdSe_2$, and $PtSe_2$ for tunable device. *ACS Appl. Nano. Mater* **1**, 1932–1939, https://doi.org/10.1021/acsanm.8b00363 (2018).

20. Qin, D. *et al.* Monolayer $PdSe_2$: A promising two-dimensional thermoelectric material. *Sci. Rep.* **8**, 2764, https://doi.org/10.1038/s41598-018-20918-9 (2018).

21. Chen, Y. *et al.* Tuning electronic structure of single layer MoS_2 through defect and interface engineering. *ACS Nano* **12**, 2569–2579, https://doi.org/10.1021/acsnano.7b08418 (2018).

22. Xu, L. *et al.* Two-dimensional MoS_2-Graphene-based multilayer van der Waals heterostructures: enhanced charge transfer and optical absorption, and electric-field tunable dirac point and band gap. *Chem. Mater.* **29**, 5504–5512, https://doi.org/10.1021/acs.chemmater.7b00281 (2017).

23. Zhao, X. W. *et al.* Spontaneous spin polarization of methanol molecule adsorbed on B- or N-doped graphene: first-principles calculations. *Eur. Phys. J. B* **92**, 90485–3, https://doi.org/10.1140/epjb/e2019-90485-3 (2019).

24. Zhang, K. H. *et al.* Tuning the electronic and photonic properties of monolayer MoS_2 via *In situ* rhenium substitutional doping. *Adv. Funct. Mater.* **28**, 1706950, https://doi.org/10.1002/adfm.201706950 (2018).

25. Cui, J. F. *et al.* Unprecedented Piezoresistance Coefficient in Strained Silicon Carbide. *Nano Lett.* **19**, 6569–657, https://doi.org/10.1021/acs.nanolett.9b02821 (2019).

26. Zhou, W. *et al.* Intrinsic structural defects in monolayer molybdenum disulfide. *Nano Lett.* **13**, 2615–2622, https://doi.org/10.1021/nl4007479 (2013).

27. Han, S. W. *et al.* Controlling ferromagnetic easy axis in a layered MoS_2 single crystal. *Phys. Rev. Lett.* **110**, 247201, https://doi.org/10.1103/PhysRevLett.110.247201 (2013).

28. Li, H. *et al.* Activating and optimizing MoS_2 basal planes for hydrogen evolution through the formation of strained sulphur vacancies. *Nat. Mater.* **15**, 48–53, https://doi.org/10.1038/nmat4465 (2016).

29. Tongay, S. *et al.* Defects activated photoluminescence in two-dimensional semiconductors: interplay between bound, charged and free excitons. *Sci. Rep.* **3**, 2657, https://doi.org/10.1038/srep02657 (2013).

30. Lin, J. H. *et al.* Novel Pd2Se$_3$ two-dimensional phase driven by interlayer fusion in layered PdSe2. *Phys. Rev. Lett* **119**, 016101, https://doi.org/10.1103/PhysRevLett.119.016101 (2017).

31. Zhu, X. R., Li, F., Wang, Y., Qiao, M. & Li, Y. F. Pd2Se$_3$ monolayer: a novel two-dimensional material with excellent electronic, transport, and optical properties. *J. Mater. Chem. C* **6**, 4494–4500, https://doi.org/10.1039/C8TC00810H (2018).

32. Nguyen, G. D. *et al.* 3D imaging and manipulation of subsurface selenium vacancies in $PdSe_2$. *Phys. Rev. Lett.* **121**, 086101, https://doi.org/10.1103/PhysRevLett.121.086101 (2018).

33. Zhang, X. *et al.* Computational Screening of 2D Materials and Rational Design of Heterojunctions for Water Splitting Photocatalysts. *Small Methods* **2**, 1700359, https://doi.org/10.1002/smtd.201700359 (2018).

34. Yuan, S., Roldán, R., Katsnelson, M. I. & Guinea, F. Effect of point defects on the optical and transport properties of MoS_2 and WS$_2$. *Phys. Rev. B* **90**, 041402, https://doi.org/10.1103/PhysRevB.90.041402 (2014).

35. Schedin, F. *et al.* Detection of individual gas molecules adsorbed on graphene. *Nat. Mater.* **6**, 652–655, https://doi.org/10.1038/nmat1967 (2007).

36. Kresse, G. & Hafner, J. Ab initio molecular dynamics for liquid metals. *Phys. Rev. B* **47**, 558, https://doi.org/10.1103/PhysRevB.47.558 (1993).

37. Kresse, G. & Furthmüller, J. Efficiency of ab-initio total energy calculations for metals and semiconductors using a plane-wave basis set. *Comp. Mater. Sci.* **6**, 15–50, https://doi.org/10.1016/0927-0256(96)00008-0 (1996).

38. Blöchl, P. E. Projector augmented-wave method. *Phys. Rev. B* **50**, 17953–17979, https://doi.org/10.1103/PhysRevB.50.17953 (1994).

39. Kresse, G. & Joubert, D. From ultrasoft pseudopotentials to the projector augmented-wave method. *Phys. Rev. B* **59**, 1758–1775, https://doi.org/10.1103/PhysRevB.59.1758 (1999).

40. Heyd, J., Scuseria, G. E. & Ernzerhof, M. Hybrid functionals based on a screened coulomb potential. *J. Chem. Phys.* **118**, 8207–8215, https://doi.org/10.1063/1.1564060 (2003).

41. Gajdoš, M., Hummer, K., Kresse, G. & Furthmüller, J. Linear optical properties in the projector-augmented wave methodology. *Phys. Rev. B* **73**, 045112, https://doi.org/10.1103/PhysRevB.73.045112 (2006).

42. Eberlein, T. *et al.* Plasmon spectroscopy of free-standing graphene films. *Phys. Rev. B* **77**, 233406–233410, https://doi.org/10.1103/PhysRevB.77.233406 (2008).

43. Luo, B., Wang, X., Tian, E., Li, G. & Li, L. Electronic structure, optical and dielectric properties of $BaTiO_3$/$CaTiO_3$/$SrTiO_3$ ferroelectric superlattices from first-principles calculations. *J. Mater. Chem. C* **3**, 8625–8633, https://doi.org/10.1039/C5TC01622C (2015).

Author contributions
X.W.Z. did the calculations and wrote the paper, Z.Y. collected the references, J.T.G. and W.W.Y. prepared the figures, G.C.H. and J.F.R. analyzed the data, X.B.Y. generated the research idea. All authors read and approved the final manuscript.

Competing interests
The authors declare no competing interests.

Additional information
Correspondence and requests for materials should be addressed to X.B.Y. or J.F.R.

Reprints and permissions information is available at www.nature.com/reprints.

Publisher's note Springer Nature remains neutral with regard to jurisdictional claims in published maps and institutional affiliations.